OCT 2 2 1981

E-10-4-15

NAS 1.60 : 1897

NASA Technical Paper 1897

Application of Information Theory to the Design of Line-Scan Imaging Systems

Friedrich O. Huck, Stephen K. Park,
Nesim Halyo, and Steven T. Stallman

SEPTEMBER 1981

NASA

42

NASA Technical Paper 1897

Application of Information Theory to the Design of Line-Scan Imaging Systems

Friedrich O. Huck and Stephen K. Park
Langley Research Center
Hampton, Virginia

Nesim Halyo and Steven T. Stallman
Information and Control Systems
Hampton, Virginia

National Aeronautics
and Space Administration

**Scientific and Technical
Information Branch**

1981

BLANK PAGE

CONTENTS

INTRODUCTION 1

DEFINITIONS, ASSUMPTIONS, AND FORMULATIONS 2
- Imaging Process 2
- Signal Characteristics 5
- Information and Data Density 7
- Information Efficiency 9

RADIANCE AND SYSTEM MODELS 11
- Radiance Field 11
- Imaging System 13

RESULTS AND CONCLUSIONS 16
- Computational Results 16
- Constraints and Conclusions 25

CONCLUDING REMARKS 27

APPENDIX - FORMULATION FOR PRACTICAL DESIGN TRADEOFF STUDIES 29

REFERENCES 31

SYMBOLS 34

BLANK PAGE

INTRODUCTION

The performance of line-scan imaging systems, such as TV cameras and optical-mechanical scanners, has received appreciable attention in the literature (refs. 1 to 14). The emphasis of these investigations usually has been on resolution, detection, recognition, identification, and accuracy of reconstruction of spatial detail. The most useful and widely accepted analysis approach that evolved from these investigations (most notably through the efforts of Schade, refs. 4 and 5) is to apply Fourier methods to the evaluation of optical imaging processes. The importance of this approach is that the MTF and noise characteristics of optical and electronic components can be measured with practical instrumentation and conveniently combined with each other to predict and evaluate the performance of electro-optical systems.

In this paper we explore information theory as a logical extension of Fourier methods to assess the performance of line-scan imaging systems, with emphasis on systems which use a digital communication link for transmitting data. Information theory is used to derive a single figure of merit that accounts for the statistical properties of the radiance field, the spatial response (PSF or MTF) and noise characteristics of the imaging system, and the effects of sampling and quantization due to the line-scan and digitization process. It treats the image that is reconstructed from the digital data as a received message which gives information about the incident radiance and accounts for degradations as loss of information.

Fellgett and Linfoot (refs. 15 and 16) first applied Shannon's (ref. 17) theory of information to the assessment of image quality. They formulated the information capacity and density of photographic images and accounted for the degradation of image quality caused by blurring and random noise. These formulations have been applied to the evaluation of photographic film by Linfoot (ref. 18), Jones (ref. 19), and Shaw (ref. 20), and of radiation detectors by Jones (ref. 21). Huck and Park (ref. 22) and Halyo and Stallman (ref. 23) extended the formulations to include performance characteristics of line-scan imaging systems by accounting for degradations caused by aliasing and quantization. Aliasing errors are generated when spatial details of the radiance field are insufficiently sampled, and quantization noise is generated when the discrete (i.e., sampled analog) signal is digitized.

These formulations based on information theory are constrained by the assumption that the signal and noise amplitudes are Gaussian, ergodic, additive, and statistically independent. Nevertheless, it is of interest to explore information as a figure of merit for assessing the performance of line-scan imaging systems and, in particular, for optimizing their efficiency to acquire and transmit information. This interest arises because the quantity of data that is transmitted and the amount of information that the data can contain are inevitably related by sampling and quantization. The relationship between

information and data suggests the concept of information efficiency (i.e., ratio of information density to data density) as a useful design criterion.

DEFINITIONS, ASSUMPTIONS, AND FORMULATIONS

Figure 1 illustrates a linear, space-invariant imaging process that converts the continuous radiance field $L(x,y)$ into a digital signal $s(x,y;X,Y;\kappa)$.

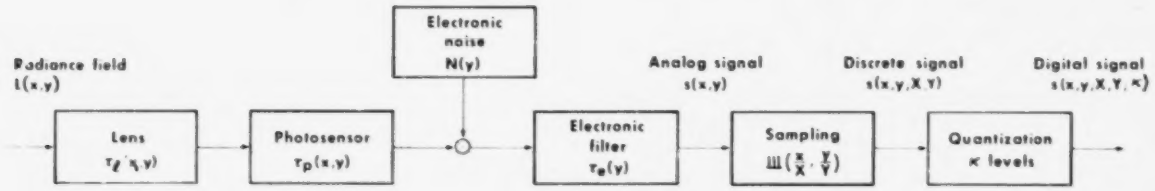

Figure 1.- Model of line-scan imaging process.

In the first of the following four subsections, we formulate the conversion of the radiance field into a discrete signal $s(x,y;X,Y)$. In the second section we define properties of the digital signal $s(x,y;X,Y;\kappa)$ that is generated when the discrete signal $s(x,y;X,Y)$ is quantized. In the third section we formulate the information and data density of the digital signal, and in the fourth section we define and discuss information efficiency.

The information density of an image that is reconstructed from discrete data is a function of the image reconstruction process as well as of the imaging system. We account for image reconstruction by a low-pass filter that coincides with the sampling passband. This reconstruction filter would be optimum - in the sense of transferring information from the output of the imaging system to the image display without loss of information - if the signal were band-limited. We do not investigate optimum reconstruction for signals that are not band-limited.

Imaging Process

The conversion of a continuous radiance field $L(x,y)$ into a discrete signal $s(x,y;X,Y)$ can be defined by the expression

$$s(x,y;X,Y) = \{K\, L(x,y) \star \tau(x,y) + N(y) \star [\delta(x)\ \tau_e(y)]\}\ \text{Ш}\left(\frac{x}{X}, \frac{y}{Y}\right) \qquad (1)$$

The function $\tau(x,y)$ is the PSF (point-spread function or spatial response) of the imaging system given by

$$\tau(x,y) = \tau_\ell(x,y) * \tau_p(x,y) * [\delta(x)\ \tau_e(y)]$$

where $\tau_\ell(x,y)$, $\tau_p(x,y)$, and $\delta(x)\ \tau_e(y)$ are the PSF's of the lens, of the spot intensity profile (for TV cameras) or photosensor aperture shape (for optical-mechanical scanners), and of the electronic filter, respectively. The steady-state gain of the conversion of radiance into the photosensor signal (see the Appendix) is denoted by K, the electronic noise by $N(y)$, convolution by $*$, and the sampling function (ref. 24) by

$$\text{Ш}\left(\frac{x}{X}, \frac{y}{Y}\right) = \sum_{m=-\infty}^{\infty} \sum_{n=-\infty}^{\infty} \delta\left(\frac{x}{X} - m, \frac{y}{Y} - n\right)$$

$$= XY \sum_{m=-\infty}^{\infty} \sum_{n=-\infty}^{\infty} \delta(x - Xm, y - Yn)$$

Rectangular (Cartesian) coordinates (x,y) in the object plane are used as reference for the imaging coordinates. The sampled signal $s(x,y;X,Y)$ is an infinite array of δ functions on a rectangular lattice with spacing X and Y in the x- and y-directions, respectively.

Salient properties of the process defined by equation (1) are often more convenient to evaluate in the frequency domain rather than in the spatial domain. We denote the functions $\hat{g}(\upsilon,\omega)$ and $g(x,y)$ as the Fourier transform pairs given by

$$\hat{g}(\upsilon,\omega) = \int_{-\infty}^{\infty}\int g(x,y) e^{-i2\pi(\upsilon x+\omega y)}\, dx\, dy$$

$$g(x,y) = \int_{-\infty}^{\infty}\int \hat{g}(\upsilon,\omega) e^{i2\pi(x\upsilon+y\omega)}\, d\upsilon\, d\omega$$

The Fourier transform of equation (1) yields

$$\hat{s}(\upsilon,\omega;X,Y) = [K\,\hat{L}(\upsilon,\omega)\;\hat{\tau}(\upsilon,\omega) + \hat{N}(\omega)\;\hat{\tau}_e(\omega)] * XY \coprod\!\!\coprod\!\!\coprod(X\upsilon, Y\omega) \tag{2a}$$

where $\hat{\tau}(\upsilon,\omega)$ is the MTF (modulation-transfer function or spatial frequency response) given by

$$\hat{\tau}(\upsilon,\omega) = \hat{\tau}_\ell(\upsilon,\omega)\;\hat{\tau}_p(\upsilon,\omega)\;\hat{\tau}_e(\omega)$$

and (from ref. 24)

$$XY \coprod\!\!\coprod\!\!\coprod(X\upsilon, Y\omega) = XY \sum_{m=-\infty}^{\infty}\sum_{n=-\infty}^{\infty} \delta(X\upsilon - m,\; Y\omega - n)$$

$$= \sum_{m=-\infty}^{\infty}\sum_{n=-\infty}^{\infty} \delta\left(\upsilon - \frac{m}{X},\; \omega - \frac{n}{Y}\right)$$

Equation (2a) can be equivalently written as

$$\hat{s}(\upsilon,\omega;X,Y) = \hat{s}(\upsilon,\omega) + \hat{s}_a(\upsilon,\omega;X,Y) \tag{2b}$$

where $\hat{s}(\upsilon,\omega)$ is the signal component prior to sampling as given by

$$\hat{s}(\upsilon,\omega) = K\,\hat{L}(\upsilon,\omega)\;\hat{\tau}(\upsilon,\omega) + N(\omega)\;\hat{\tau}_e(\omega) \tag{3}$$

and $\hat{s}_a(\upsilon,\omega;X,Y)$ represents the sideband components of $\hat{s}(\upsilon,\omega;X,Y)$ that are generated by sampling as given by

$$\hat{s}_a(\upsilon,\omega;X,Y) = \sum_{\substack{m=-\infty \\ (m,n)\neq(0,0)}}^{\infty}\sum_{n=-\infty}^{\infty} \hat{s}\left(\upsilon - \frac{m}{X},\; \omega - \frac{n}{Y}\right) \tag{4}$$

We use the inverse Fourier transform of the frequency passband of the sampling lattice with spacing (X,Y), or briefly the sampling passband, as the reconstruction function. The sampling passband is given by the rectangle function (ref. 24)

$$\Pi(X\upsilon, Y\omega) = \begin{cases} 1 & \left(|\upsilon| < \frac{1}{2X},\ |\omega| < \frac{1}{2Y}\right) \\ 0 & \text{(elsewhere)} \end{cases}$$

The corresponding reconstruction $r(x,y)$ is the inverse Fourier transform of

$$\hat{r}(\upsilon,\omega) = \hat{s}(\upsilon,\omega;X,Y)\ \Pi(X\upsilon, Y\omega)$$

as given by

$$r(x,y) = \sum_{m=-\infty}^{\infty} \sum_{n=-\infty}^{\infty} s(mX,nY)\ \mathrm{sinc}\left(\frac{x - mX}{X}\right) \mathrm{sinc}\left(\frac{y - nY}{Y}\right)$$

where $s(mX,nY)$ is the value of $s(x,y;X,Y)$ given by equation (1).

Signal Characteristics

We assume that the radiance $L(x,y)$ and the noise $N(y)$ are independent Gaussian random (stochastic) processes and designate their Wiener spectra as $\hat{\Phi}_L(\upsilon,\omega)$ and $\hat{\Phi}_N(\omega)$, respectively. We treat quantization noise as if it were additive "white" Gaussian noise with a Wiener spectrum $\hat{\Phi}_q(K)$. The Wiener spectrum $\hat{\Phi}_s(\upsilon,\omega;X,Y;K)$ of the digital signal $\hat{s}(\upsilon,\omega;X,Y;K)$ can then be expressed as

$$\hat{\Phi}_s(\upsilon,\omega;X,Y;K) = \hat{\Phi}_s(\upsilon,\omega) + \hat{\Phi}_a(\upsilon,\omega;X,Y) + \hat{\Phi}_n(\omega;Y) + \hat{\Phi}_q(K) \tag{5}$$

The term $\hat{\Phi}_s(\upsilon,\omega)$, which represents the signal component centered at the location $(\upsilon,\omega) = (0,0)$, is given by

$$\hat{\Phi}_s(\upsilon,\omega) = K^2\ \hat{\Phi}_L(\upsilon,\omega)\ |\hat{\tau}(\upsilon,\omega)|^2 \tag{6}$$

This term accounts for image degradation due to blurring caused by loss of small detail when the higher spatial frequency components of the radiance field are attenuated by the MTF of the imaging system.

The term $\hat{\Phi}_a(\upsilon,\omega;X,Y)$, which represents the signal sideband components generated by sampling and centered at the locations $(\upsilon,\omega) = \left(\frac{m}{X}, \frac{n}{Y}\right)$, with $(m,n) \neq (0,0)$, is given by

$$\hat{\Phi}_a(\upsilon,\omega;X,Y) = \sum_{\substack{m=-\infty \\ (m,n)\neq(0,0)}}^{\infty} \sum_{n=-\infty}^{\infty} \hat{\Phi}_s\left(\upsilon - \frac{m}{X}, \omega - \frac{n}{Y}\right) \tag{7}$$

This term accounts for image degradation due to aliasing caused by masking of spatial detail when displaced spatial frequency components from the sampling sidebands intrude into the image reconstruction passband.

The term $\hat{\Phi}_n(\omega;Y)$, which represents the sampled electronic noise at the filter output, is given by

$$\hat{\Phi}_n(\omega;Y) = \sum_{n=-\infty}^{\infty} \hat{\Phi}_N\left(\omega - \frac{n}{Y}\right) \left|\hat{\tau}_e\left(\omega - \frac{n}{Y}\right)\right|^2 \tag{8}$$

It should be noted that just as undersampling of the signal frequency spectrum generates aliasing, undersampling of the noise frequency spectrum generates additional noise.

To model the effective noise generated by the quantization process, we assume that (1) the discrete signal $s(x,y;X,Y)$ is linearly quantized into K levels over the effective range $2c\sigma_s$, so that the quantum levels have a uniform spacing of $2c\sigma_s/K$, where

$$\sigma_s^2 = K^2 \iint_{-\infty}^{\infty} \hat{\Phi}_L(\upsilon,\omega)\, d\upsilon\, d\omega = K^2\sigma_L^2$$

is the maximum variance of the signal $\hat{s}(\upsilon,\omega)$ among all $\hat{\tau}(\upsilon,\omega)$ such that $|\hat{\tau}(\upsilon,\omega)| \leq 1$, and c is a constant to be determined later; (2) the quantization error of any one sample is uncorrelated with that of any other sample; and (3) the signal is equally likely to occur anywhere in the quantization interval $-c\sigma_s/\kappa$ to $c\sigma_s/\kappa$. These assumptions imply that the quantization error n_κ has the uniform probability density function (refs. 25 to 27)

$$p(n_\kappa) = \begin{cases} \dfrac{\kappa}{2c\sigma_s} & \left(\dfrac{-c\sigma_s}{\kappa} \leq n_\kappa \leq \dfrac{c\sigma_s}{\kappa}\right) \\ 0 & \text{(elsewhere)} \end{cases}$$

In fact, a random variable that is constrained to a finite interval has a maximum entropy when its probability density function is uniform. A signal with the uniform probability density function $p(n_\kappa)$ has a mean equal to zero and a variance given by

$$\sigma_q^2 = \int_{-c\sigma_s/\kappa}^{c\sigma_s/\kappa} n_\kappa^2 \, p(n_\kappa) \, dn_\kappa = \frac{1}{3}\left(\frac{c\sigma_s}{\kappa}\right)^2$$

Since quantization noise is uncorrelated (in the spatial domain), it has a Wiener spectrum equal to its variance; that is,

$$\hat{\Phi}_q(\upsilon,\omega;\kappa) = \hat{\Phi}_q(\kappa) = \sigma_q^2 = \frac{1}{3}\left(\frac{c\sigma_s}{\kappa}\right)^2 \tag{9}$$

Information and Data Density

Let A denote a rectangular (isoplanatism) patch centered at $x = y = 0$. For M line scans and N samples per scan in A, x and y are limited to

$$\frac{-XM}{2} < x < \frac{XM}{2} \qquad \frac{-YN}{2} < y < \frac{YN}{2}$$

and the area of A is $|A| = XYMN$. Any function $g(x,y)$ is then said to be confined to A if $g(x,y) = 0$ for all points outside A. Furthermore, let

the spatial function $g(x,y)$ be a second-order, stationary, Gaussian random process that is effectively band-limited to the sampling passband $\Pi(X\upsilon, Y\omega)$.[1] Following Shannon (ref. 17), we can define the statistical uncertainty of this process, or the quantity of information contained in the area A (ref. 15), to be (refs. 22 and 23)

$$H_g = \frac{1}{2}|A| \int_{-1/2X}^{1/2X} \int_{-1/2Y}^{1/2Y} \log_2 [4\pi \hat{\Phi}_g(\upsilon,\omega)] \, d\upsilon \, d\omega$$

The units of H_g are binits.

The information gained about patch A of a scene can be regarded as a reduction in the uncertainty of the probable state of that patch. In this sense, it can be shown that the amount of information H_i that is gained is (refs. 22 and 23)

$$H_i = \frac{1}{2}|A| \int_{-1/2X}^{1/2X} \int_{-1/2Y}^{1/2Y} \log_2 [4\pi \hat{\Phi}_s(\upsilon,\omega;X,Y;\kappa)] \, d\upsilon \, d\omega$$

$$- \frac{1}{2}|A| \int_{-1/2X}^{1/2X} \int_{-1/2Y}^{1/2Y} \log_2 \{4\pi[\hat{\Phi}_a(\upsilon,\omega;X,Y)$$

$$+ \hat{\Phi}_n(\omega;Y) + \hat{\Phi}_q(\kappa)]\} \, d\upsilon \, d\omega$$

where $\hat{\Phi}_s(\upsilon,\omega;X,Y;\kappa)$ is the Wiener spectrum of the digital signal as given by equation (5). This formulation is permitted because the additive terms in equation (5) are statistically independent. The information density, or entropy, of the digital signal can thus be formulated as (refs. 22 and 23)

---

[1] No attempt is made to investigate the optimization of reconstruction filters.

$$h_i = \frac{H_i}{|A|} = \frac{1}{2} \int_{-1/2X}^{1/2X} \int_{-1/2Y}^{1/2Y} \log_2 \left[1 + \frac{\hat{\Phi}_s(\upsilon,\omega)}{\hat{\Phi}_a(\upsilon,\omega;X,Y) + \hat{\Phi}_n(\omega;Y) + \hat{\Phi}_q(\kappa)} \right] d\upsilon \, d\omega \qquad (10)$$

where $\hat{\Phi}_s(\upsilon,\omega)$, $\hat{\Phi}_a(\upsilon,\omega;X,Y)$, $\hat{\Phi}_n(\omega;Y)$, and $\hat{\Phi}_q(\kappa)$ are given by equations (6) to (9). The units of h_i are binits per square meter.

Each discrete signal $s(x,y;X,Y)$ is quantized into κ levels. Thus, the number of distinguishable states in patch A is κ^{MN}, and the amount of data in A is

$$H_d = MN \log_2 \kappa = \frac{|A|}{XY} \log_2 \kappa$$

The units of H_d are bits. The data density for η-bit encoding, $\kappa = 2^\eta$, is

$$h_d = \frac{H_d}{|A|} = \frac{1}{XY} \log_2 \kappa = \frac{\eta}{XY} \qquad (11)$$

The units of h_d are bits per square meter.

Information Efficiency

We define the ratio h_i/h_d as the information efficiency of the digital image data. This definition of information efficiency is analogous to Khinchin's definition of "relative entropy" as the ratio $h/\log m$, where h is the entropy of a test and $\log m$ is the maximum value of h for the m different symbols of the test (ref. 28). Another analogy is Jones' definition of "information efficiency" of a beam of light as the information capacity per transmitted photon (ref. 29).

However, to properly interpret the information efficiency h_i/h_d, we must account for an important difference between continuous and discrete entropies (ref. 17). The data density h_d is defined for a discrete random variable (i.e., quantization levels with a uniform probability density function) for which the entropy provides an absolute measure of randomness. The information density h_i is defined for a continuous random variable (i.e., an analog signal with a Gaussian probability density function) for which the entropy provides a measure of randomness relative to an assumed standard (namely, the coordinate system chosen with each small spatial element $dx\,dy$ given equal weight). It would be intuitively satisfying to adjust the ratio h_i/h_d so that the theoretical upper limit of information efficiency becomes unity. This upper limit is reached for the following three conditions:

1. The Wiener spectrum of the radiance field $L(x,y)$ is constant within the sampling passband; that is,

$$\hat{\Phi}_L(\upsilon,\omega) = \begin{cases} \sigma_L^2 & \left(|\upsilon| < \frac{1}{2X},\ |\omega| < \frac{1}{2Y}\right) \\ 0 & \text{(elsewhere)} \end{cases}$$

This condition represents maximum entropy within the sampling passband.

2. The imaging system has the (unrealizable) MTF

$$\hat{\tau}(\upsilon,\omega) = \begin{cases} 1 & \left(|\upsilon| < \frac{1}{2X},\ |\omega| < \frac{1}{2Y}\right) \\ 0 & \text{(elsewhere)} \end{cases}$$

This condition prevents aliasing and blurring within the sampling passband.

For these two conditions, equation (10) reduces to the expression

$$h_i = \frac{1}{2XY} \log_2 \left(1 + \frac{\sigma_s^2}{\sigma_n^2 + \sigma_q^2}\right) \tag{12}$$

where $\sigma_s^2 = K^2\sigma_L^2$ is the maximum possible variance of the signal and σ_n^2 and σ_q^2 are the variances of the electronic and quantization noise, respectively.

3. The quantization intervals are very large compared with the magnitude of the electronic noise fluctuations (i.e., $\sigma_q >> \sigma_n$). Substituting equation (9) for σ_q^2 further reduces equation (12) to

$$h_i = \frac{1}{2XY} \log_2 \left(1 + \frac{\sigma_s^2}{\sigma_q^2}\right)$$

$$= \frac{1}{2XY} \log_2 \left(1 + \frac{3K^2}{c^2}\right) \approx \frac{1}{XY} \log_2 \frac{\sqrt{3}K}{c} \tag{13}$$

It follows by comparison of equation (13) for h_i with equation (11) for the data density h_d that the information efficiency h_i/h_d is unity if $c = \sqrt{3}$. This adjustment of the upper limit of the information efficiency h_i/h_d to unity leads to a linear encoding of the Gaussian signal variation over a dynamic range of $-\sqrt{3}\sigma_s$ to $\sqrt{3}\sigma_s$, which encompasses 92 percent of the signal.

If, instead of the third condition, we assume that the quantization interval is very small compared with the magnitude of the electronic noise fluctuations (i.e., $\sigma_q << \sigma_n$) or that the analog signal is not quantized (i.e., $\sigma_q = 0$), the expression for h_i given by equation (12) reduces to

$$h_i = \frac{1}{2XY} \log_2 \left(1 + \frac{\sigma_s^2}{\sigma_n^2} \right) \tag{14}$$

This expression may be recognized as Shannon's channel capacity with an average power limitation (ref. 17).

A basic assumption in formulations of the entropy of signals transmitted through a communication channel is that the frequency of these signals can be sufficiently band-limited. The limiting rate of information transmission (i.e., channel capacity) is reached for this condition when the signals approximate, in statistical properties, white noise (Shannon's theorem 17). However, a space-varying radiance field generally cannot be sufficiently band-limited by the response of optical systems prior to line-scan sampling, so that aliasing caused by insufficient sampling must be accounted for. Herein lies a basic difference between formulations of information acquired by line-scan imaging systems and formulations of information transmitted through communication channels (ref. 17) or acquired by photographic film (refs. 15, 16, and 18 to 20) and radiation detectors (ref. 21).

RADIANCE AND SYSTEM MODELS

Radiance Field

We assume that the radiance field $L(x,y)$ is both homogeneous and isotropic, so that the variance of $L(x,y)$ is independent of (x,y) and the autocovariance (and autocorrelation) are functions only of the relative distance (ref. 30)

$$r = [(x_1 - x_2)^2 + (y_1 - y_2)^2]^{1/2}$$

between points (x_1,y_1) and (x_2,y_2). Furthermore, we assume that the autocovariance of $L(x,y)$ is

$$\Phi_L K(r) = \sigma_L^2 e^{-r/\mu_r} \tag{15}$$

so that the associated Wiener spectrum, which is the circularly symmetric Fourier transform (i.e., the Hankel transform) of $\Phi_L(r)$, is

$$\hat{\Phi}_L(\upsilon,\omega) = \hat{\Phi}_L(\rho) = \frac{2\pi\mu_r^2\sigma_L^2}{[1 + (2\pi\mu_r\rho)^2]^{3/2}} \tag{16}$$

where $\rho^2 = \upsilon^2 + \omega^2$ (see fig. 2).

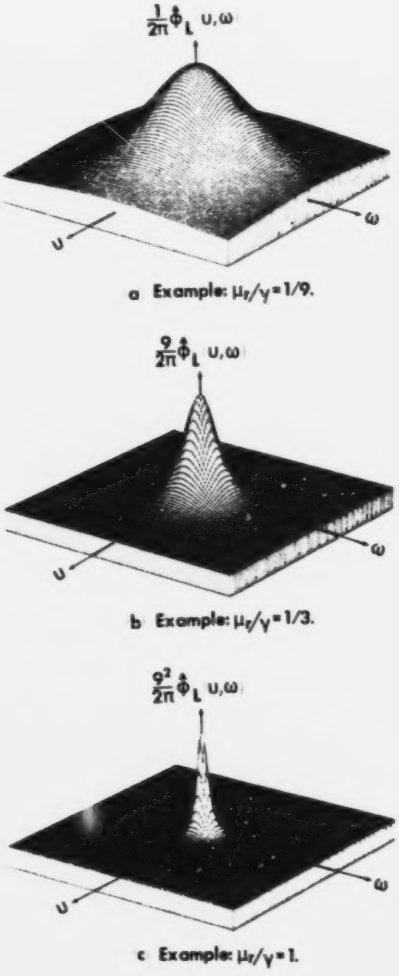

Figure 2.- Wiener spectrum of radiance field.

Equation (16) can be derived by assuming that $L(x,y)$ is a random set of two-dimensional pulses whose width r obeys the Poisson probability density function with the (expected) mean width u_r and whose magnitude obeys the Gaussian probability density function with the (expected) mean u_L and variance σ_L^2 (refs. 31 and 32). The variance σ_L^2 and the Wiener spectrum $\hat{\Phi}_L(\upsilon,\omega)$ are related by

$$\sigma_L^2 = \Phi_L(0) = \int_{-\infty}^{\infty}\int \hat{\Phi}_L(\upsilon,\omega)\, d\upsilon\, d\omega$$

$$= 2\pi \int_0^{\infty} \rho\, \hat{\Phi}_L(\rho)\, d\rho \qquad (17)$$

that is, σ_L^2 is the value of the integrated Wiener spectrum.

Imaging System

The conversion of radiance into a discrete signal involves some sort of photon detection and sampling mechanism. The most common mechanisms are TV cameras and optical-mechanical scanners. In this paper we disregard the MTF of the objective lens, so that the MTF $\hat{\tau}(\upsilon,\omega)$ of the imaging system (see fig. 1) reduces to

$$\hat{\tau}(\upsilon,\omega) = \hat{\tau}_p(\upsilon,\omega)\ \hat{\tau}_e(\omega)$$

where $\hat{\tau}_p(\upsilon,\omega)$ is the MTF of the spot intensity of TV cameras or of the photosensor aperture of optical-mechanical scanners; $\hat{\tau}_e(\omega)$ is the MTF of the electronic filter; and ω is the spatial frequency component in the line-scan direction. The sampling interval X represents the distance between successive line scans, and the interval Y represents the product of the line-scan rate and the time between electronic samples. (There is, of course, no electronic sampling in commercial TV; the signal that is generated along the line-scan direction is transmitted as an analog signal.)

Figure 3 illustrates salient characteristics of one spot intensity profile and two photosensor aperture shapes. The profile and apertures are of equivalent size; that is,

$$\int_{-\infty}^{\infty}\int \tau_p(x,y)\, dx\, dy = \hat{\tau}_p(0,0) = 1$$

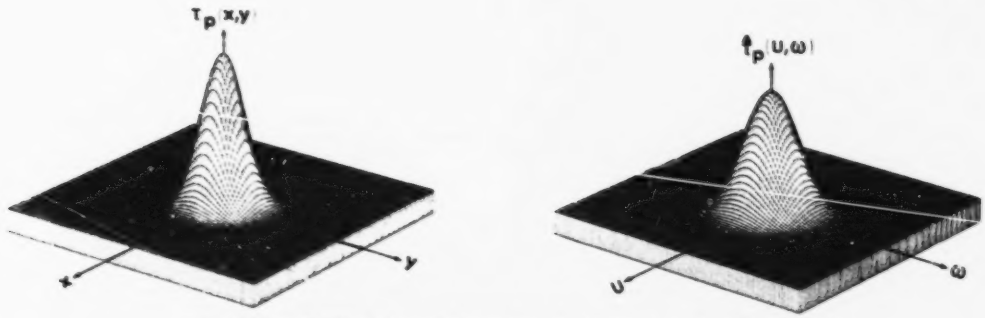

(a) PSF and MTF of Gaussian spot intensity (with equivalent diameter γ).

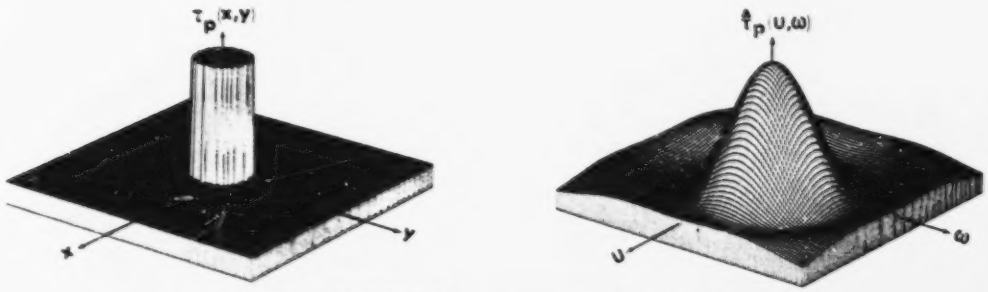

(b) PSF and MTF of circular photosensor aperture (with diameter γ).

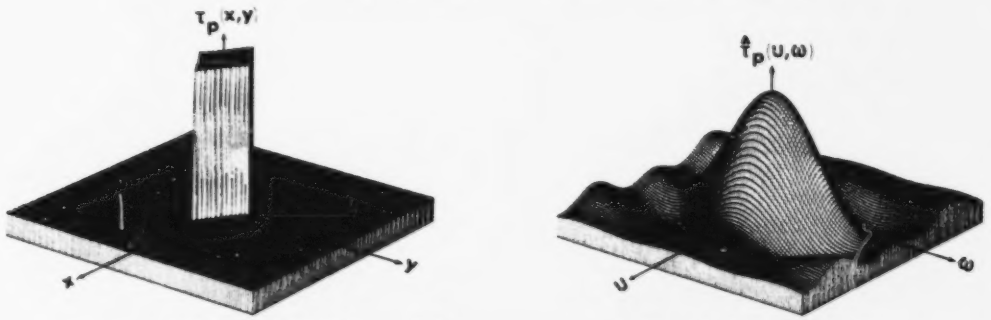

(c) PSF and MTF of diamond photosensor aperture (with equivalent diameter γ).

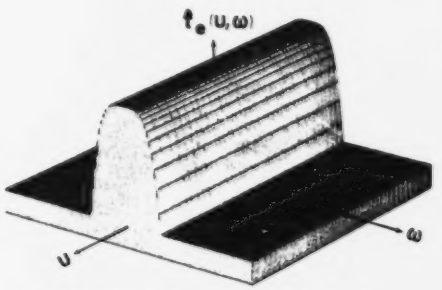

(d) MTF of electronic filter (for $\Upsilon = \gamma$).

Figure 3.- Properties of photon-detection mechanisms.

It follows that $\tau_p(0,0) = 4/\pi\gamma^2$ for the Gaussian spot intensity, and

$$\tau_p(x,y) = \begin{cases} \dfrac{4}{\pi\gamma^2} & ((x,y) \in \text{aperture area}) \\ 0 & (\text{elsewhere}) \end{cases}$$

for the circular and diamond photosensor apertures. It is convenient to regard the diameter γ of the circular aperture also as the equivalent diameter of the Gaussian spot intensity and diamond aperture, that is, as the equivalent diameter of the PSF of the photon-detection mechanism. The MTF's $\hat{\tau}_p(\upsilon,\omega)$ are given by the following expressions:

(a) Gaussian:

$$\hat{\tau}_p(\upsilon,\omega) = \hat{\tau}_p(\rho) = e^{-(\pi\gamma\rho/2)^2} \tag{18}$$

(b) Circular:

$$\hat{\tau}_p(\upsilon,\omega) = \hat{\tau}_p(\rho) = \frac{J_1(\pi\gamma\rho)}{\pi\gamma\rho/2} \tag{19}$$

(c) Diamond:

$$\hat{\tau}_p(\upsilon,\omega) = \operatorname{sinc} \frac{1}{2}\left(\frac{\pi\gamma\upsilon}{2} + \gamma\omega\right) \operatorname{sinc} \frac{1}{2}\left(\frac{\pi\gamma\upsilon}{2} - \gamma\omega\right) \tag{20}$$

Mertz and Gray (ref. 1) were the first to observe that reasonable spot intensity profiles and photosensor aperture shapes of equivalent size result in about equal blurring but that some profiles and shapes suppress aliasing better than others. Schade (refs. 4 and 5), in particular, has shown that the Gaussian intensity profile illustrated in figure 3(a) is advantageous for suppressing aliasing, providing that sufficient overlap exists between successive line scans.

The shape of the photosensor aperture in optical-mechanical scanners is commonly circular, as illustrated in figure 3(b), or rectangular. To obtain a response $\tau_p(x,y)$ that is similar to the Gaussian profile would require shading of the aperture with a variable transmittance profile. However, this would be extremely difficult, since these apertures are typically less than a millimeter across. Instead, as shown by Katzberg et al. (ref. 9), it is possible to accomplish a similar effect by shaping the aperture, that is, by

adjusting the width of the aperture to follow some curve which then adjusts the υ spatial frequency response normal to the line-scan direction. The exact aperture shape along the line-scan direction is less important, since the effective ω spatial frequency response can be reshaped by an electronic low-pass filter. To demonstrate the improvement that can be attained with photosensor aperture shaping, we choose the diamond shape illustrated in figure 3(c). This diamond shape has already been shown (refs. 1, 9, 14, and 23) to be superior (in suppressing aliasing) to the circular shape.

For the electronic frequency response we select the function given by

$$\hat{\tau}_e(\omega) = \begin{cases} 1 - (2Y\omega)^4 & (|\omega| < 1/2Y) \\ 0 & (|\omega| > 1/2Y) \end{cases} \tag{21}$$

and plotted in figure 3(d). The cutoff frequency $1/2Y$ ensures sufficient sampling (i.e., a Nyquist sampling rate) of the analog signal (and noise) generated along the line-scan direction.

RESULTS AND CONCLUSIONS

Computational Results

Computational results shown in figures 4 and 5 account only for the blurring and aliasing caused by the PSF and sampling process of line-scan photon-detection mechanisms, whereas results shown in figures 6 and 7 account, in addition, for the degradations caused by electronic noise and quantization. By accounting first only for blurring and aliasing, we establish upper limits for the information density that can be attained with the photon-detection mechanisms evaluated in this investigation. The inclusion of electronic noise and quantization leads to the assessment of practical systems.

Results are presented as a function of normalized parameters to account for a wide range of conditions. The Wiener spectrum $\hat{\Phi}_L(\upsilon,\omega)$ of the radiance field given by equation (16) is normalized as

$$\hat{\Phi}'_L(\upsilon,\omega) = \sigma_L^{-2}\,\hat{\Phi}_L(\upsilon,\omega)$$

where σ_L^2 is the variance of the radiance field given by equation (17). The mean spatial width u_r of the radiance field and the sampling intervals X and Y of the imaging system are normalized by the equivalent diameter γ of the PSF's. For example, for the circular aperture with γ its actual diameter, $X/\gamma = Y/\gamma = 1$ represents contiguous coverage, and $u_r/\gamma = 1$ represents mean spatial detail equal to the diameter of the projection of the aperture, or its IFOV, onto the scene.

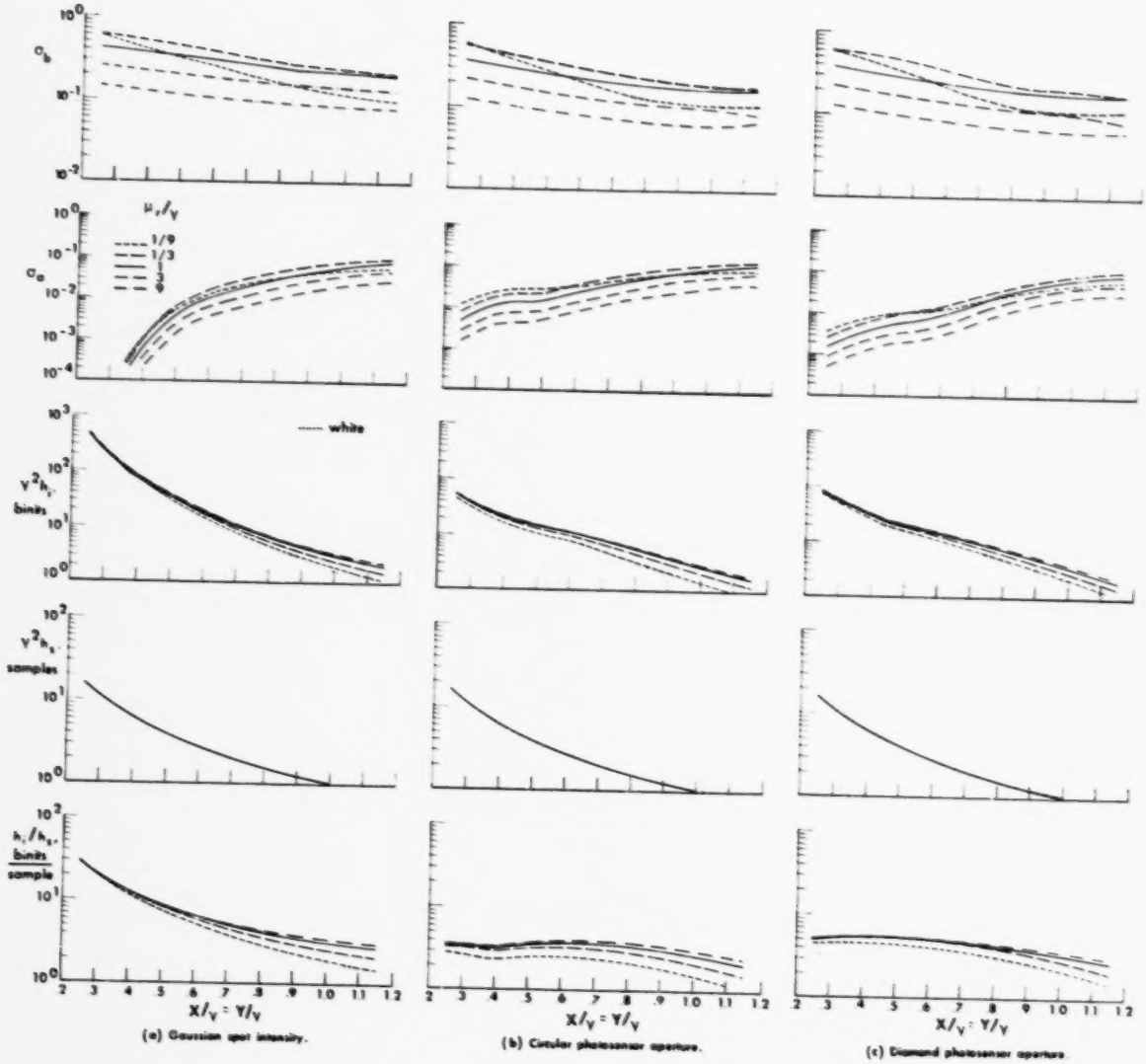

Figure 4.- Variation of blurring σ_b, aliasing σ_a, information density h_i, sampling density h_s, and information per sample h_i/h_s vs sampling intervals $X = Y$ for several mean spatial widths u_r of the radiance field. h_i and h_i/h_s include curves for a ("white") Wiener spectrum that remains constant with frequency.

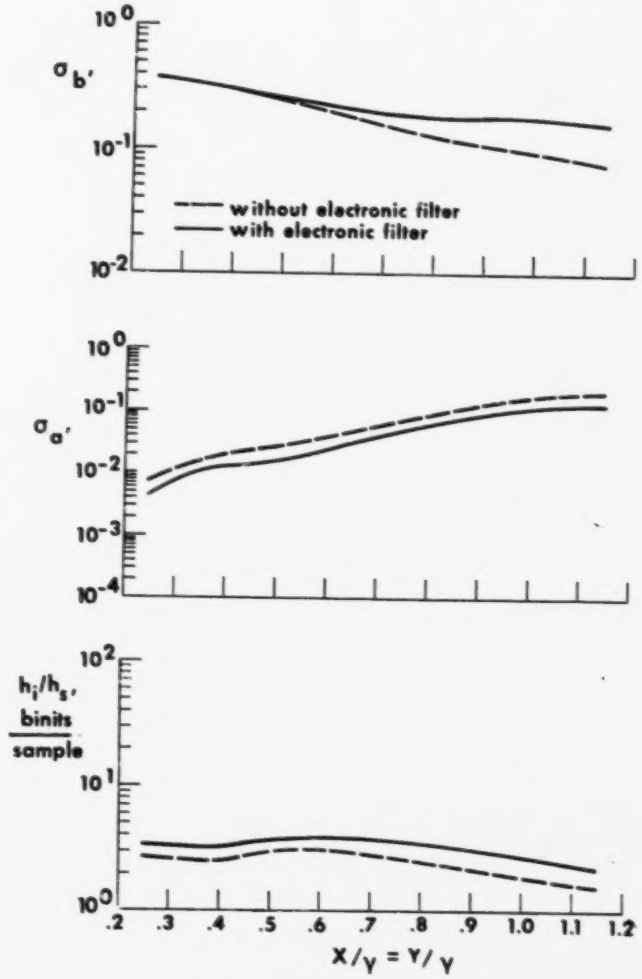

Figure 5.- Variation of blurring σ_b, aliasing σ_a, and information per sample h_i/h_s vs sampling intervals X = Y for a circular photosensor aperture with and without electronic filter.

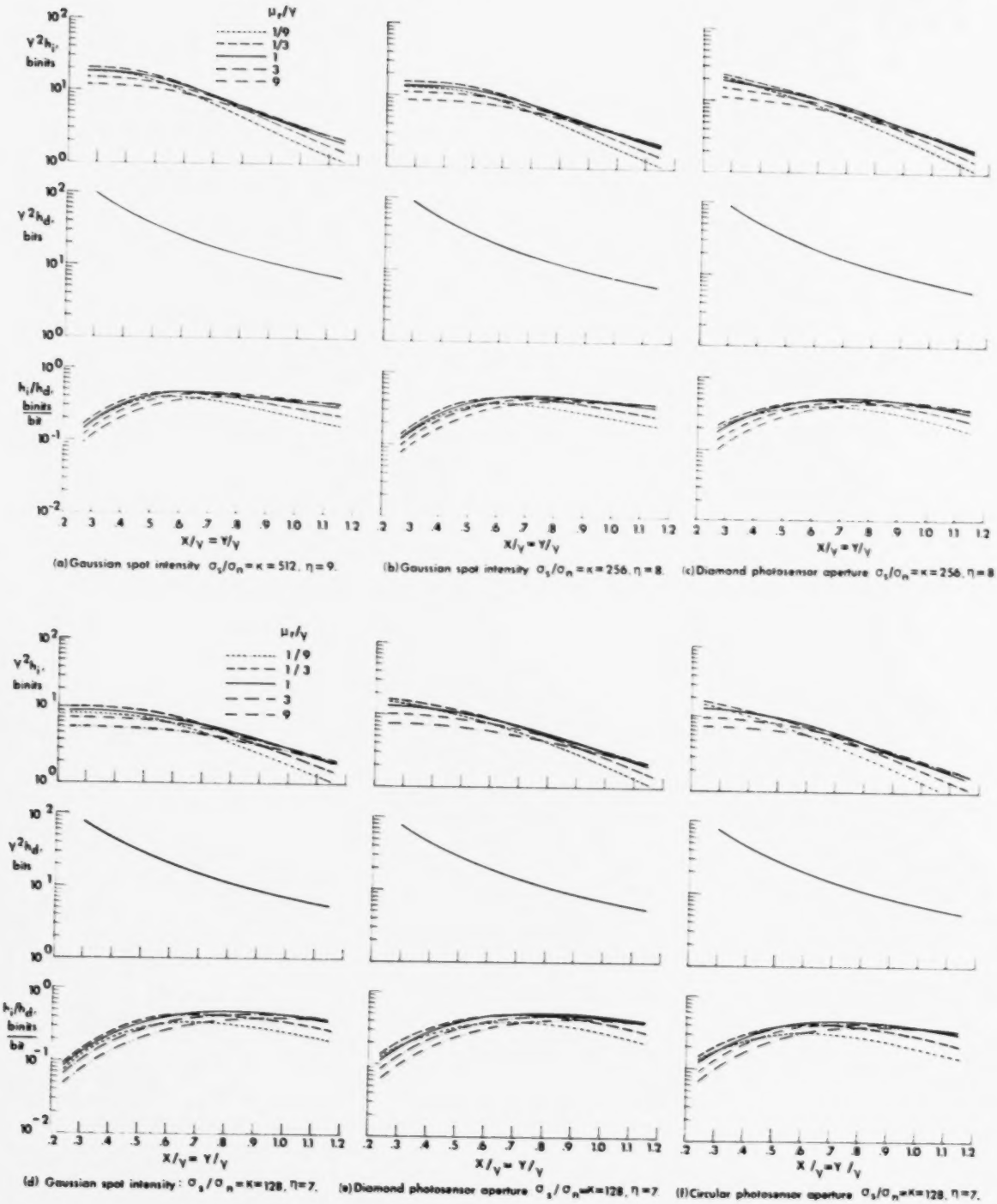
μ_r/Y
1/9
1/3
1
3
9
$Y^2 h_i$, bits
$Y^2 h_d$, bits
h_i/h_d, bits/bit
X/Y = Y/Y
(a) Gaussian spot intensity $\sigma_s/\sigma_n = \kappa = 512$, $\eta = 9$.
(b) Gaussian spot intensity $\sigma_s/\sigma_n = \kappa = 256$, $\eta = 8$.
(c) Diamond photosensor aperture $\sigma_s/\sigma_n = \kappa = 256$, $\eta = 8$
(d) Gaussian spot intensity: $\sigma_s/\sigma_n = \kappa = 128$, $\eta = 7$.
(e) Diamond photosensor aperture $\sigma_s/\sigma_n = \kappa = 128$, $\eta = 7$.
(f) Circular photosensor aperture $\sigma_s/\sigma_n = \kappa = 128$, $\eta = 7$.

Figure 6.- Variation of information density h_i, data density h_d, and information efficiency h_i/h_d vs sampling intervals X = Y for several mean spatial widths μ_r of the radiance field.

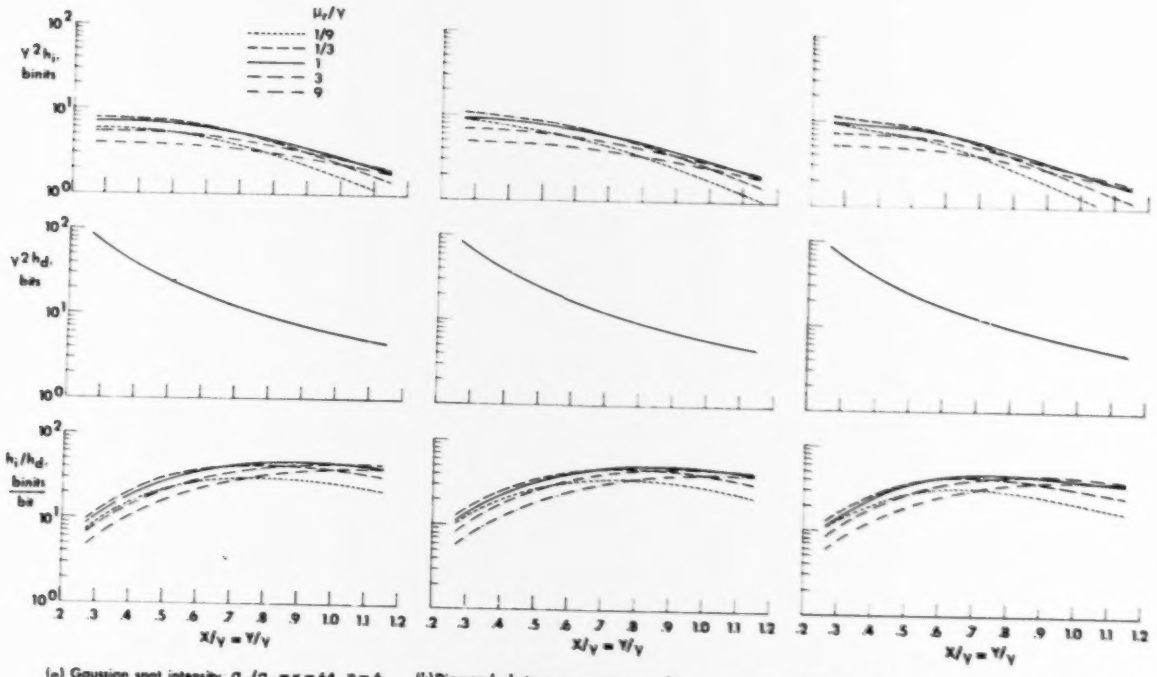

(g) Gaussian spot intensity $\sigma_s/\sigma_n = \kappa = 64$, $\eta = 6$. (h) Diamond photosensor aperture $\sigma_s/\sigma_n = \kappa = 64$, $\eta = 6$. (i) Circular photosensor aperture $\sigma_s/\sigma_n = \kappa = 64$, $\eta = 6$.

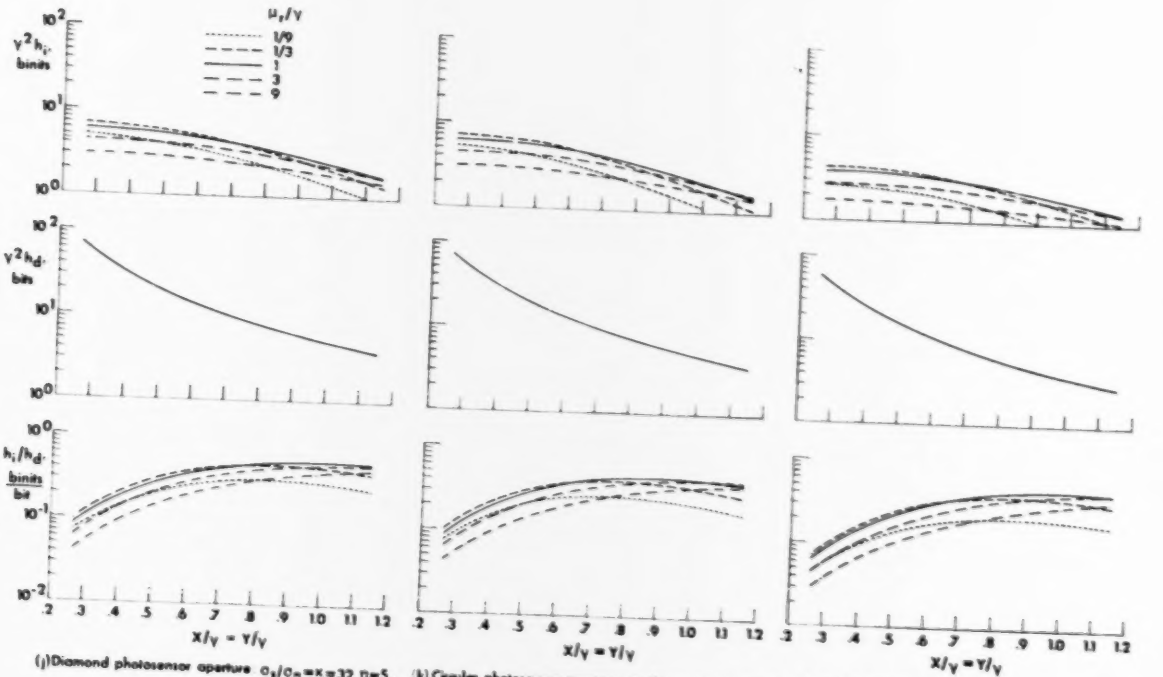

(j) Diamond photosensor aperture $\sigma_s/\sigma_n = \kappa = 32$, $\eta = 5$. (k) Circular photosensor aperture $\sigma_s/\sigma_n = \kappa = 32$, $\eta = 5$. (l) Circular photosensor aperture $\sigma_s/\sigma_n = \kappa = 16$, $\eta = 4$.

Figure 6.- Concluded.

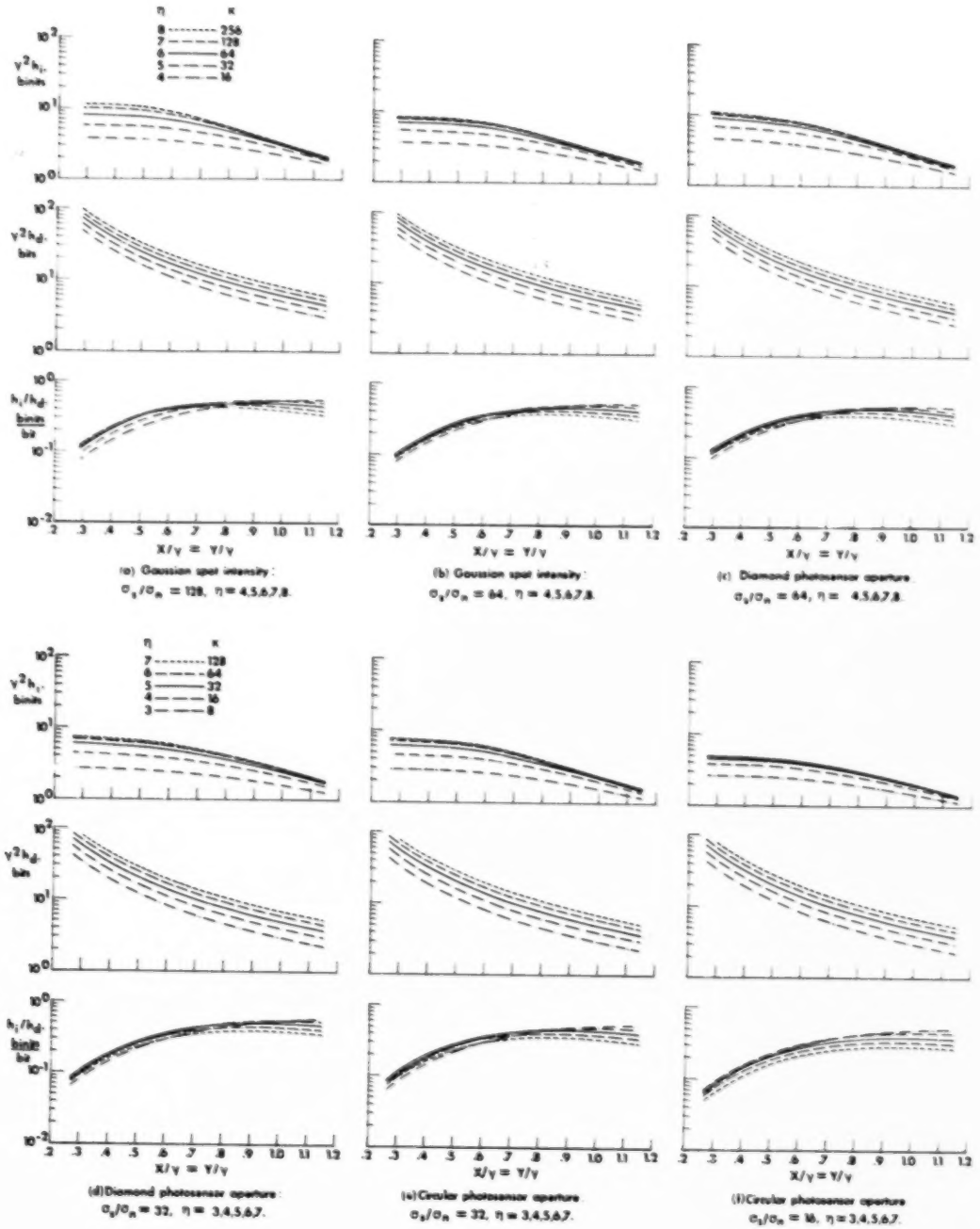

Figure 7.- Variation of information density h_i, data density h_d, and information efficiency h_i/h_d vs sampling intervals $X = Y$ for several encoding levels η. Mean width u_r of the radiance field is equal to the equivalent diameter γ of the PSF.

Image degradation due to blurring is characterized by the (normalized) variance σ_b^2 as computed by (ref. 23)

$$\sigma_b^2 = \int_{-1/2Y}^{1/2Y} \int_{-1/2X}^{1/2X} \hat{\Phi}_L'(\upsilon,\omega) \left|1 - \hat{\tau}(\upsilon,\omega)\right|^2 d\upsilon\, d\omega \tag{22}$$

Blurring occurs when the higher frequency components of the radiance field are attenuated by the MTF $\hat{\tau}(\upsilon,\omega)$ of the imaging system within the sampling passband; for example, $\sigma_b^2 = 0$ if $\hat{\tau}(\upsilon,\omega) = \Pi(X\upsilon, Y\omega)$. Fellgett and Linfoot (ref. 15) refer to the degradation defined by equation (22) as fidelity defect due to loss of sharpness. Figures 4 and 5 present curves of the standard deviation σ_b which show how blurring increases with decreasing sampling intervals. This increase in blurring occurs because the (fixed) MTF $\hat{\tau}(\upsilon,\omega)$ of the imaging system becomes an increasing source of degradation of the signal frequency components that could otherwise be reconstructed as the sampling passband $\Pi(X\upsilon, Y\omega)$ increases. This effect is particularly pronounced for small spatial detail (i.e., $u_r/\gamma < 1/3$).

Image degradation due to aliasing is characterized by the (normalized) variance σ_a^2 as computed by

$$\sigma_a^2 = \int_{-1/2Y}^{1/2Y} \int_{-1/2X}^{1/2X} \sum_{\substack{m=\infty \\ (m,n)\neq(0,0)}}^{\infty} \sum_{n=\infty}^{\infty} \hat{\Phi}_L'\left(\upsilon - \frac{m}{X}, \omega - \frac{n}{Y}\right) \left|\hat{\tau}\left(\upsilon - \frac{m}{X}, \omega - \frac{n}{Y}\right)\right|^2 d\upsilon\, d\omega \tag{23}$$

Aliasing occurs because displaced spatial frequency components from the sampling sidebands intrude into the sampling passband; for example, $\sigma_a^2 = 0$ if $\hat{\tau}(\upsilon,\omega) = \Pi(X\upsilon, Y\omega)$. Figures 4 and 5 present curves of the standard deviation σ_a which show how aliasing decreases with decreasing sampling intervals. This decrease in aliasing occurs because the Wiener spectrum $\hat{\Phi}_L(\upsilon,\omega)\left|\hat{\tau}(\upsilon,\omega)\right|^2$ decreases with frequency and because the distance between sampling sidebands (as observed in the frequency domain) increases as $\left(\frac{1}{X}, \frac{1}{Y}\right)$, whereas the sampling passband increases only as $\left(\frac{1}{2X}, \frac{1}{2Y}\right)$.

It should be noted that blurring is only weakly dependent on differences between the PSF of the spot intensity and photosensor apertures, whereas aliasing is strongly dependent on these differences, as has already been observed in a number of previous investigations (refs. 1, 4, 5, 9, 14, and 23). The

Gaussian profile and diamond shape are both superior (in suppressing aliasing) to the circular shape at broad sampling intervals ($X/\gamma = Y/\gamma > 0.5$), and the Gaussian profile is appreciably superior to both aperture shapes at narrow sampling intervals ($X/\gamma = Y/\gamma < 0.5$). These differences in performance are directly attributable to their MTF characteristics shown in figure 3.

The information density h_i, analogous to equation (10) but without electronic noise and quantization, is computed as

$$h_i = \frac{1}{2} \int_{-1/2X}^{1/2X} \int_{-1/2Y}^{1/2Y} \log_2 \left[1 + \frac{\hat{\Phi}'_L(\upsilon,\omega) \, |\hat{\tau}(\upsilon,\omega)|^2}{\sum_{\substack{m=-\infty \\ (m,n)\neq(0,0)}}^{\infty} \sum_{n=-\infty}^{\infty} \hat{\Phi}'_L\left(\upsilon - \frac{m}{X}, \omega - \frac{n}{Y}\right) \left|\hat{\tau}\left(\upsilon - \frac{m}{X}, \omega - \frac{n}{Y}\right)\right|^2} \right] d\upsilon \, d\omega \qquad (24)$$

The corresponding sampling density h_s is

$$h_s = \frac{1}{XY} \qquad (25)$$

The units of h_i are binits per γ^2, and of h_s are samples per γ^2. Figure 4 presents curves of the information density h_i, sampling density h_s, and the ratio h_i/h_s vs sampling intervals. The units of h_i/h_s are binits per sample.

The curves in figure 4 were obtained for Wiener spectra that decrease with spatial frequency as formulated by equation (16); in addition, h_i and h_i/h_s are also given for a ("white") Wiener spectrum that remains constant with frequency. It can be observed that the curves of h_i and h_i/h_s for various mean spatial details approach each other as these details become larger until it becomes difficult to distinguish the curves from each other (at the scale of the drawing). This suggests that the curves for $\mu_r/\gamma = 9$ approach upper limits of h_i and h_i/h_s for the assumed conditions. On the other extreme, as the mean spatial detail becomes smaller than $\mu_r/\gamma = 1/9$, the Wiener spectrum becomes increasingly constant with frequency (within the MTF passband of the imaging system), and curves of h_i and h_i/h_s approach those for a white Wiener spectrum.

The range of information per sample h_i/h_s is remarkably narrow for the wide range of Wiener spectra that has been considered. Since these curves do not include degradation due to electronic noise and quantization, they represent an upper limit of the information per sample that can be reached with line-scan photon-detection mechanisms for the assumed Wiener spectra and the PSF's.

Figure 5 shows results for the circular photosensor aperture with and without the electronic filter. The latter condition represents an optical-mechanical scanner design in which the IFOV is stepped at discrete intervals along the y-direction rather than scanned in a continuous motion; that is, the radiance field is spatially sampled in the y-direction as well as the x-direction. The effect of the electronic filter (for continuous line scans) is to increase blurring and decrease aliasing; the net effect is an improvement in information per sample of about 30 to 45 percent, depending on sampling intervals. This improvement represents an approximate upper limit that can be attained with electronic filters, since the assumed filter MTF ensures sufficient sampling along the y-axis. (Small changes in the response of this filter, by changing the exponent in eq. (21) from 4 to either 2 or 8, have little effect; a change to 2 increases blurring and decreases aliasing, and a change to 8 has the opposite effect; the effect on information per sample is negligible.)

Results shown in figures 6 and 7 account for image degradations due to electronic noise and quantization as well as blurring and aliasing. The information density h_i is computed using the approximation of equation (10) given by

$$h_i = \frac{1}{2} \int_{-1/2X}^{1/2X} \int_{-1/2Y}^{1/2Y} \log_2 \left[1 + \frac{\hat{\Phi}'_L(\upsilon,\omega)\ |\hat{\tau}(\upsilon,\omega)|^2}{\sum_{\substack{m=-\infty \\ (m,n)\neq(0,0)}}^{\infty} \sum_{n=-\infty}^{\infty} \hat{\Phi}'_L\left(\upsilon - \frac{m}{X}, \omega - \frac{n}{Y}\right) \left|\hat{\tau}\left(\upsilon - \frac{m}{X}, \omega - \frac{n}{Y}\right)\right|^2 + \left(\frac{\sigma_s}{\sigma_n}\right)^{-2} + K^{-2}} \right] d\upsilon\, d\omega \qquad (26)$$

The ratio σ_s/σ_n is a convenient parameter for characterizing the electronic signal but is not the conventional rms SNR. Here, σ_s^2 is the maximum variance of the signal $\hat{s}(\upsilon,\omega)$ among all $\hat{\tau}(\upsilon,\omega)$ such that $|\hat{\tau}(\upsilon,\omega)| \leq 1$, given by

$$\sigma_s^2 = K^2 \sigma_L^2$$

and σ_n^2 is the variance of the electronic noise at the output of the electronic filter, given by

$$\sigma_n^2 = \int_{-1/2Y}^{1/2Y} \hat{\Phi}_N(\omega;Y)\ |\hat{\tau}_e(\omega)|^2\, d\omega$$

(Further details are given in the Appendix.) The corresponding data density is given by equation (11) as

$$h_d = \frac{1}{XY} \log_2 \kappa = \frac{\eta}{XY}$$

where η is the number of bits used to encode the κ quantization levels.

Both figures 6 and 7 present plots of the variation of information density h_i, data density h_d, and information efficiency h_i/h_d with sampling intervals. Figure 6 characterizes performance as a function of mean spatial detail u_r of the radiance field for several ratios σ_s/σ_n and encoding levels η that have been selected so that the rms magnitudes of electronic and quantization noise are equal to each other. Figure 7 characterizes performance as a function of encoding levels η for several ratios σ_s/σ_n and a fixed mean spatial detail u_r equal to the equivalent diameter γ of the PSF's.

Statistical properties of the radiance field, such as mean spatial detail or Wiener spectrum, are seldom known in practice. Therefore, it often becomes appropriate to regard each set of curves (for different values of u_r/γ) in figure 6 as boundaries that encompass typical performance.

Constraints and Conclusions

Time versus spatial response.- When Shannon's theory of information transmitted through communication channels is applied to the formulation of information acquired with line-scan imaging systems, differences between time (electronic) and spatial (optical) MTF's must be taken into account. A time-varying signal can be sufficiently band-limited by practical electronic filters to reduce aliasing to an insignificant source of degradation. Formulations of information transmitted through communication channels have, partly for this reason, been based on the assumption of band-limited signals. However, formulations of information acquired with line-scan imaging systems cannot be simplified by this assumption. The realizability of MTF shapes of optical filters is constrained by the fact that their (sensitivity or transmittance) response can never be negative. This constraint leads to MTF's that tend to diminish very gradually with frequency, generally without a finite cutoff (except for lens diffraction). These responses insufficiently band-limit the radiance field prior to line-scan sampling, a condition which tends to result in significant degradation due to aliasing. The inclusion of aliasing leads to significant departures in the performance characteristics of line-scan imaging systems from those of communication channels.

Continuous versus discrete entropy.- Formulations of the information density of digital image data are subject to a somewhat arbitrary normalization of the (continuous) Gaussian signal variations relative to the (discrete) linear quantization intervals. We have adjusted the formulation of information density for computational purposes so that the theoretical upper limit of information efficiency reaches unity. This adjustment results in a linear dynamic range that encompasses 92 percent of the (assumed) Gaussian signal distribution.

Information density versus spatial detail.- The information density of discrete and digital data (figs. 4 and 6, respectively) varies comparatively little with large variations in the mean spatial detail of the random radiance field. For variations of the mean spatial detail by nearly 2 orders of magnitude (from 1/9 to 9 times the equivalent diameter of the PSF), the information density varies by less than a factor of 3. This occurs because the small spatial detail associated with high entropies is subject to more degradation due to aliasing and blurring than the large spatial detail associated with low entropies.

Information efficiency versus sampling intervals.- Information efficiency of discrete data exhibits a distinct single maximum when displayed as a function of sampling intervals (figs. 6 and 7). The location and magnitude of this maximum depend on the properties of the radiance field, the PSF and sensitivity of the photon-detection mechanism, and the number of encoding levels. Designs favorable to maximum information efficiency have the following characteristics:

$\sigma_s/\sigma_n = \kappa$	Sampling interval (X/Y = Y/Y) for -		
	Gaussian	Diamond	Circular
512	0.6	---	---
256	0.6 to 0.7	0.6 to 0.7	---
128	0.7	0.7	0.6 to 0.7
64	0.7 to 0.8	0.7 to 0.8	0.7
32	---	0.8	0.7 to 0.8
16	---	---	0.7 to 0.8

Sampling intervals narrower than those listed in this table will improve information density if the radiance field consists mostly of spatial detail equal to or smaller than the PSF, while broader sampling intervals will generally reduce both information density and efficiency.

PSF versus spatial detail.- For sampling intervals favorable for maximum information efficiency, information density and efficiency both tend to be maximum when the PSF of the imaging system is approximately equal to the mean spatial detail of the radiance field (fig. 6). This result is consistent with the earlier discussion about the conditions that lead to the theoretical upper limit of information efficiency. These conditions require that the MTF and sampling passband be matched to the Wiener spectrum of the scene.

Kell factor.- Sampling intervals favorable for maximum information efficiency compare closely with the so-called Kell factor that evolved from early studies (refs. 2 and 3) concerned with the selection of a line-scan interval (or line pitch) for commercial TV cameras and displays. The Kell factor is a measure of the number of lines required to distinguish between black and white bars oriented parallel to the line-scan direction. According to Kell et al. (ref. 3), "The average of readings made by several observers indicated that

100 scanning lines were required to make 64 black and white bars distinguishable." This result led to a Kell factor of 0.64. The concept of Kell factor was readily accepted but not its numerical value. Baldwin (ref. 2) lists the results of six different investigations, including his own, with values ranging from 0.53 to 0.85 and an average of 0.71. However, it should be noted that the Kell factor defines the line-scan interval relative to bar targets with widths approximately equal to the PSF of the TV camera, whereas we define 2-D sampling intervals relative to the equivalent diameter of the PSF itself and use random rather than periodic targets.

Schade's recommendation.- Schade (refs. 4, 5, and in ref. 7), in extensive and widely recognized studies of TV systems, defines line-scan intervals as a function of the MTF of the imaging system. His recommendation for a lower and upper limit on the line-scan interval, expressed in our notation, is

$$\frac{1}{2\upsilon\hat{}_{\tau=0.05}} \leq X/\gamma \leq \frac{1}{2\upsilon\hat{}_{\tau=0.4}}$$

where $\upsilon\hat{}_{\tau=0.05}$ and $\upsilon\hat{}_{\tau=0.4}$ are the frequencies at which the MTF normal to the line-scan direction is 0.05 and 0.4, respectively. For the photon-detection mechanisms considered in this paper, this recommendation results in $0.44 \leq X/\gamma \leq 0.83$ for the Gaussian spot intensity, $0.49 \leq X/\gamma \leq 0.78$ for the diamond photosensor aperture, and $0.44 \leq X/\gamma \leq 0.63$ for the circular photosensor aperture.

Quantization versus electronic noise.- Information density ceases to increase significantly with increasing quantization levels when the number of quantization levels κ exceeds the rms signal-to-noise ratio σ_s/σ_n. Information efficiency begins to decrease significantly with increasing quantization levels when κ exceeds $4\sigma_s/\sigma_n$. Thus, the relationship between number of quantization levels and rms signal-to-noise ratio should be such that $\sigma_s/\sigma_n < \kappa < 4\sigma_s/\sigma_n$. This conclusion, however, is strongly dependent on the assumption that was made about the (linear) dynamic range of the imaging system with respect to the (Gaussian) probability distribution of the magnitude of the radiance field.

CONCLUDING REMARKS

By tying together the statistical properties of the radiance field and the spatial response (PSF or MTF), sensitivity, and sampling and quantization intervals of the imaging system into a single figure of merit, information theory provides an obviously attractive approach for optimizing the performance of line-scan imaging systems for a specific application, especially if this application includes digital data transmission. Although the information content of the image that has been reconstructed from the digital data cannot be directly measured with practical instrumentation for an objective experimental evaluation, the component and system MTF and noise characteristics required to com-

pute information content are routinely measured. The Wiener spectrum of scenes can also be measured but is often unknown.

Optimum information density and efficiency require that the MTF and sampling passband match the Wiener spectrum of the radiance field. Computational results for statistical properties of natural radiance fields and the responses of common imaging mechanisms indicate that information density and efficiency are not strongly sensitive to variations in typical statistical properties of the radiance field and that the best performance is approached when the sampling intervals are about 0.5 to 0.7 times the equivalent diameter of the PSF. These results are consistent with the experimental and theoretical results obtained by earlier investigators concerned with the performance and design of TV cameras.

Langley Research Center
National Aeronautics and Space Administration
Hampton, VA 23665
July 6, 1981

APPENDIX

FORMULATION FOR PRACTICAL DESIGN TRADEOFF STUDIES

In this appendix we express the information density h_i formulated by equation (10) in terms of parameters that are commonly used in practice and provide details about the approximations that were made for equation (26), which was used to generate computational results.

The formulation of equation (1) is simplified by separating the spectral and spatial dependence of the radiance field and imaging system response, with the parameter K accounting for the spectral characteristics. Actually, both the radiance field and the system response are wavelength dependent, and the spatial convolution should therefore be integrated over wavelength (ref. 23). However, following common practice it is convenient here to let K be the steady-state gain of the conversion of the radiance into the photosensor signal as given by

$$K = \left(\frac{\pi}{4}\right)^2 D^2 \gamma^2 \int_0^\infty L(\lambda)\ \tau(\lambda)\ d\lambda \tag{A1}$$

where D is the lens aperture diameter, γ is the equivalent diameter of the PSF (or IFOV) formed by the spot intensity or photosensor aperture, $L(\lambda)$ and $\tau(\lambda)$ are the spectral properties of the radiance field and system response, respectively, and λ is wavelength.

The Wiener spectrum of the photosensor signal, sampling sidebands, and electronic noise given by equations (6), (7), and (8), respectively, can be rewritten as

$$\hat{\Phi}_s(\upsilon,\omega) = K^2\sigma_L^2\ \hat{\Phi}'_L(\upsilon,\omega)\ \left|\hat{\tau}(\upsilon,\omega)\right|^2 \tag{A2}$$

$$\hat{\Phi}_a(\upsilon,\omega;X,Y) = K^2\sigma_L^2 \sum_{\substack{m=-\infty \\ (m,n)\neq(0,0)}}^{\infty} \sum_{n=-\infty}^{\infty} \hat{\Phi}'_L\left(\upsilon - \frac{m}{X},\ \omega - \frac{n}{Y}\right) \left|\hat{\tau}\left(\upsilon - \frac{m}{X},\ \omega - \frac{n}{Y}\right)\right|^2 \tag{A3}$$

and

$$\hat{\Phi}_n(\omega;Y) = \sigma_N^2 \sum_{n=-\infty}^{\infty} \hat{\Phi}_N'\left(\omega - \frac{n}{Y}\right) \left|\hat{\tau}_e\left(\omega - \frac{n}{Y}\right)\right|^2 \tag{A4a}$$

The prime denotes a normalized quantity, and σ_L^2 and σ_N^2 are the variances of the radiance field and electronic noise, respectively. If the electronic filter MTF $\hat{\tau}_e(\omega)$ sufficiently band-limits the electronic noise, then equation (A4a) can be reduced to

$$\hat{\Phi}_n(\omega;Y) = \sigma_N^2 \, \hat{\Phi}_N'(\omega) \, |\hat{\tau}_e(\omega)|^2 \tag{A4b}$$

Substituting equations (A2), (A3), (A4b), and (9) into equation (10) yields

$$h_j = \frac{1}{2} \int_{-1/2X}^{1/2X} \int_{-1/2Y}^{1/2Y} \log_2 \left[1 + \frac{\hat{\Phi}_L'(\upsilon,\omega) \, |\hat{\tau}(\upsilon,\omega)|^2}{\sum\limits_{\substack{m=\infty \\ (m,n)\neq(0,0)}}^{\infty} \sum_{n=-\infty}^{\infty} \hat{\Phi}_L'\left(\upsilon - \frac{m}{X}, \omega - \frac{n}{Y}\right) \left|\hat{\tau}\left(\upsilon - \frac{m}{X}, \omega - \frac{n}{Y}\right)\right|^2 + \left(\frac{\sigma_N}{K\sigma_L}\right)^2 \hat{\Phi}_N'(\omega) \, |\hat{\tau}_e(\omega)|^2 + \frac{c^2K^{-2}}{3}} \right] d\upsilon \, d\omega \tag{A5}$$

Equation (A5) reduces to equation (26) for $c^2 = 3$, $\sigma_s = K\sigma_L$, and

$$\sigma_n^2 = \sigma_N^2 \int_{-1/2Y}^{1/2Y} \hat{\Phi}_N'(\omega) \, |\hat{\tau}_e(\omega)|^2 \, d\omega$$

The (normalized) Wiener spectrum $\hat{\Phi}_N'(\omega)$ of the electronic noise tends to either remain constant or to decrease with frequency, and the MTF of the low-pass electronic filter $\hat{\tau}_e(\omega)$ usually remains nearly constant out to some frequency near the sampling passband and then decreases rapidly. Consequently, $\sigma_n \lesssim \sigma_N$.

REFERENCES

1. Mertz, P.; and Gray, F.: Theory of Scanning and Its Relation to Characteristics of Transmitted Signal in Telephotography and Television. Bell Syst. Tech. J., vol. 13, no. 3, July 1934, pp. 464-515.

2. Baldwin, Millard W., Jr.: The Subjective Sharpness of Simulated Television Images. Bell Syst. Tech. J., vol. XIX, no. 4, Oct. 1940, pp. 563-586.

3. Kell, R. D.; Bedford, A. V.; and Fredendall, G. L.: A Determination of Optimum Number of Lines in a Television System. RCA Rev., vol. V, no. 1, July 1940, pp. 8-30.

4. Schade, Otto H.: Image Gradation, Graininess and Sharpness in Television and Motion Picture Systems.
   Part I: Image Structure and Transfer Characteristics. J. SMPTE, vol. 56, no. 2, Feb. 1951, pp. 137-177.
   Part II: The Grain Structure of Motion Picture Images - An Analysis of Deviations and Fluctuations of the Sample Number. J. SMPTE, vol. 58, no. 3, Mar. 1952, pp. 181-222.
   Part III: The Grain Structure of Television Images. J. SMPTE, vol. 61, no. 2, Aug. 1953, pp. 97-164.
   Part IV, A & B: Image Analysis in Photographic and Television Systems (Definition and Sharpness). J. SMPTE, vol. 64, no. 11, Nov. 1955, pp. 593-617.

5. Schade, Otto H., Sr.: An Evaluation of Photographic Image Quality and Resolving Power. J. SMPTE, vol. 73, no. 2, Feb. 1964, pp. 81-119.

6. Callahan, L. G.; and Brown, W. M.: One- and Two-Dimensional Processing in Line Scanning Systems. Appl. Opt., vol. 2, no. 4, Apr. 1963, pp. 401-407.

7. Macovski, A.: Spatial and Temporal Analysis of Scanned Systems. Appl. Opt., vol. 9, no. 8, Aug. 1970, pp. 1906-1910.

8. Biberman, Lucien M., ed.: Perception of Displayed Information. Plenum Press, Inc., c.1973.

9. Katzberg, Stephen J.; Huck, Friedrich O.; and Wall, Stephen D.: Photosensor Aperture Shaping To Reduce Aliasing in Optical-Mechanical Line-Scan Imaging Systems. Appl. Optics, vol. 12, no. 5, May 1973, pp. 1054-1060.

10. Robinson, A. H.: Multidimensional Fourier Transforms and Image Processing With Finite Scanning Apertures. Appl. Opt., vol. 12, no. 10, Oct. 1973, pp. 2344-2352.

11. Pearson, D. E.: Transmission and Display of Pictorial Information. John Wiley & Sons, Inc., 1975.

12. Gonsalves, Robert A.; and Considine, Philip S.: Spot Shaping and Incoherent Optical Smoothing for Raster Scanned Imagery. Opt. Eng., vol. 15, no. 1, Jan./Feb. 1976, pp. 64-67.

13. Pratt, William K.: Digital Image Processing. John Wiley & Sons, Inc., c.1978.

14. Huck, Friedrich O.; Park, Stephen K.; Halyo, Nesim; and Stallman, Steven T.: Aliased Noise in Radiometric Measurements. NASA TP-1639, 1980.

15. Fellgett, P. B.; and Linfoot, E. H: On the Assessment of Optical Images. Phil. Trans. Roy. Soc. London, ser. A, vol. 247, no. 931, Feb. 17, 1955, pp. 369-407.

16. Linfoot, E. H.: Information Theory and Optical Images. J. Opt. Soc. America, vol. 45, no. 10, Oct. 1955, pp. 808-819.

17. Shannon, C. E.: A Mathematical Theory of Communication. Bell Syst. Tech. J., vol. XXVII, no. 3, July 1948, pp. 379-423.

18. Linfoot, E. H.: Equivalent Quantum Efficiency and the Information Content of Photographic Images. J. Photogr. Sci., vol. 9, 1961, pp. 188-194.

19. Jones, R. Clark: Information Capacity of Photographic Films. J. Opt. Soc. America, vol. 51, no. 11, Nov. 1961, pp. 1159-1171.

20. Shaw, Rodney, ed.: Selected Readings in Image Evaluation. Waverly Press, Inc., c.1976.

21. Jones, R. Clark: Information Capacity of Radiation Detectors. J. Opt. Soc. America, vol. 50, no. 12, Dec. 1960, pp. 1166-1170.

22. Huck, Friedrich O.; and Park, Stephen K.: Optical-Mechanical Line-Scan Imaging Process: Its Information Capacity and Efficiency. Appl. Opt., vol. 14, no. 10, Oct. 1975, pp. 2508-2520.

23. Halyo, Nesim; and Stallman, Steven T.: A Parametric Study of Aliasing Error for a Narrow Field of View Scanning Radiometer. NASA CR-3294, 1980.

24. Bracewell, Ron: The Fourier Transform and Its Applications. McGraw-Hill Book Co., Inc., c.1965.

25. Bennett, W. R.: Spectra of Quantized Signals. Bell Syst. Tech. J., vol. XXVII, no. 3, July 1948, pp. 446-472.

26. Halyo, N.; and McAlpine, G. A.: A Discrete Model for Product Quantization Errors in Digital Filters. IEEE Trans. Audio & Electroacoust., vol. AU-19, no. 3, Sept. 1971, pp. 255-256.

27. Carlson, A. Bruce: Communication Systems. McGraw-Hill Book Co., c.1968.

28. Khinchin, A. I. (R. A. Silverman and M. D. Friedman, transl.): Mathematical Foundations of Information Theory. Dover Publ., Inc., c.1957.

29. Jones, R. Clark: Information Capacity of a Beam of Light. J. Opt. Soc. America, vol. 52, no. 5, May 1962, pp. 493-501.

30. Rosenfeld, Azriel; and Kak, Avinash C.: Digital Picture Processing. Academic Press, Inc., 1976.

31. Takagi, T.; and Tutumi, S.: Statistical Properties of Radiance Spatial Distribution of Sky and Forest Backgrounds. Electron. & Commun. Japan, vol. 51, no. 2, Feb. 1968, pp. 82-90.

32. Itakura, Yasumasa; Tsutsumi, Suteo; and Takagi, Tohru: Statistical Properties of the Background Noise for the Atmospheric Windows in the Intermediate Infrared Region. Infrared Phys., vol. 14, no. 1, Feb. 1974, pp. 17-29.

SYMBOLS

A	rectangular isoplanatism patch
$\|A\|$	area of rectangular patch, m^2
c	constant that relates range of signal fluctuations to range of quantization
$g(x,y)$	spatial function
$\hat{g}(\upsilon,\omega)$	spatial frequency spectrum of $g(x,y)$, m^2
h_d	data density, bits/m^2
h_i	information density, binits/m^2
h_i/h_d	information efficiency, binits/bit
h_s	sampling density, samples/m^2
H_d	quantity of data in A, bits
H_i	quantity of information about A in digital data, binits
$J_1(\cdot)$	first-order Bessel function
K	steady-state gain of the conversion of radiance into electronic signal, $A\text{-}W^{-1}$
$L(x,y)$	radiance field, $W\text{-}m^{-2}$
m,n	sampling counts along x- and y-axes, respectively
$N(y)$	electronic noise, A
r^2	$= x^2 + y^2$
$r(\cdot)$	reconstructed image, A
$s(\cdot)$	signal, A
x,y	imaging coordinates, m
X,Y	sampling intervals, m
γ	equivalent diameter of the point-spread function of the photon-detection mechanism (i.e., of the Gaussian spot intensity and the circular and diamond photosensor aperture), m

$\delta(x,y)$	two-dimensional unit impulse function, m^{-2}
η	number of binary encoding levels, bits
κ	number of quantization levels
λ	wavelength, m
u_r	(expected) mean value of spatial widths of radiance field, m
ρ^2	$= \upsilon^2 + \omega^2$
σ	standard deviation, $W\text{-}m^{-2}$
$\tau(x,y)$	point-spread function (PSF) or spatial response
$\hat{\tau}(\upsilon,\omega)$	modulation-transfer function (MTF) or spatial frequency response
υ,ω	spatial frequencies along x- and y-axes, respectively, m^{-1} (cycles-m^{-1})
$\Phi(\cdot)$	autocovariance, $W^2\text{-}m^{-4}$
$\hat{\Phi}(\cdot)$	Wiener (or power density) spectrum, $W^2\text{-}m^{-2}$ ($W^2\text{-}m^{-4}/cycles^2\text{-}m^{-2}$)
$\Pi(\cdot)$	spatial frequency passband of sampling lattice, m^{-2} (cycles/m^2)
$\underline{\vert\vert\vert}(\cdot)$	sampling function
*	convolution
^	frequency domain
'	(prime) normalized quantity

Subscripts:

a	aliased noise, or sidebands generated by sampling
b	blurring
e	electronic filter
ℓ	lens
L	radiance field
n	electronic noise at filter output
N	electronic noise at filter input
p	photosensor aperture or spot intensity

q	quantization
s	analog signal (without noise)

1. Report No.	2. Government Accession No.	3. Recipient's Catalog No.
NASA TP-1897		

4. Title and Subtitle	5. Report Date
APPLICATION OF INFORMATION THEORY TO THE DESIGN OF LINE-SCAN IMAGING SYSTEMS	September 1981
	6. Performing Organization Code 506-61-53-06
7. Author(s)	8. Performing Organization Report No.
Friedrich O. Huck, Stephen K. Park, Nesim Halyo, and Steven T. Stallman	L-14542
9. Performing Organization Name and Address	10. Work Unit No.
NASA Langley Research Center Hampton, VA 23665	11. Contract or Grant No.
12. Sponsoring Agency Name and Address	13. Type of Report and Period Covered
National Aeronautics and Space Administration Washington, DC 20546	Technical Paper
	14. Sponsoring Agency Code

15. Supplementary Notes

Friedrich O. Huck and Stephen K. Park: Langley Research Center.
Nesim Halyo and Steven T. Stallman: Information and Control Systems, Hampton, Va.

16. Abstract

Information theory is used to formulate a single figure of merit for assessing the performance of line-scan imaging systems as a function of their spatial response (point-spread function (PSF) or modulation transfer function (MTF)), sensitivity, sampling and quantization intervals, and the statistical properties of a random radiance field. Computational results for the information density and efficiency (i.e., the ratio of information density to data density) are intuitively satisfying and compare well with experimental and theoretical results obtained by earlier investigators concerned with the performance of TV systems.

17. Key Words (Suggested by Author(s))	18. Distribution Statement
Information theory Electro-optical systems	Unclassified - Unlimited Subject Category 35

19. Security Classif. (of this report)	20. Security Classif. (of this page)	21. No. of Pages	22. Price
Unclassified	Unclassified	39	A03

For sale by the National Technical Information Service, Springfield, Virginia 22161

NASA-Langley, 1981